Comparison of Compressible and Incompressible CFD Methods for the Acoustic Analysis of Flow Induced Noise in Confined Flow

Natalie Witkowski[1], Andreas Hueppe[1], Manfred Kaltenbacher[1]

[1] *Institute of Mechanics and Mechatronics, Vienna University of Technology, Email: natalie.witkowski@tuwien.ac.at*

Abstract

Obtrusions such as bends, constrictions and junctions occurring in confined flows give rise to turbulent flow structures and separation zones. The acoustic analysis of the flow-induced noise may be accomplished using two different approaches. The first is the highest modeling approach, wherein the full set of compressible Navier Stokes equations is solved. Difficulties lie in the amplitude disparities between the acoustic and flow pressures, with differences of up to seven orders of magnitude. More favored is the hybrid approach. Based on an initial flow calculation comprising of either compressible or incompressible Navier Stokes formulations, acoustic source terms may be computed. With use of acoustic analogies, such as the Lighthill acoustic analogy or the perturbation ansatz, a subsequent acoustic analysis may be performed. The purpose of this research is to compare results of the acoustic analysis obtained by compressible and incompressible fluid simulations with focus on the identification and quantification of acoustically relevant flow structures.

Introduction

Turbulent flow structures such as vortices or separation zones, and their interaction with the mechanical environment act as acoustic sources, which lead to acoustic wave propagation through the system. The investigated geometry combines flow obtrusions to varying degrees, see Figure 1.

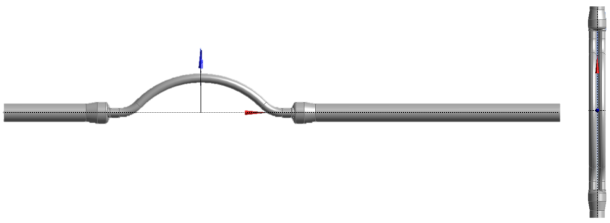

Figure 1: A front and top view of the investigated geometry.

The acoustic effect is most prominent at high flow rates, and thus four high flow speeds were investigated with Reynolds numbers 700.000, 1.100.000, 1.452.000 and 1.828.000 with the flow medium specified as air at 10 bar and 20 °C. It is expected that the main acoustic sources will be present at the junctions, bends and diameter changes, since it is at these positions that the main velocity changes, pressure changes and turbulences will be produced.

Acoustic Analogies

There are two methods with which the aeroacoustic quantities of the system may be deduced. The first, more complicated method, is to solve the full set of compressible Navier Stokes equations where both the fluid and acoustic quantities are resolved simultaneously. This method is both time and resource consuming, since it must be ensured that the small acoustic quantities, which can be up to several orders of magnitude smaller than the flow quantities, are accurately resolved [1]. The pressure quantity that results from this method is a combination of the flow and acoustic pressures.

The second method is the hybrid approach. In this approach, the fluid dynamics of the system are resolved first. Thereafter, with the help of acoustic analogies, the acoustic source terms of the system may be deduced and the acoustic computation performed [1]. This method has its advantages in that when the flow is solved as incompressible, the acoustic quantities are obtained separately from the flow quantities und thus may be studied as a separate entity. This is useful when trying to understand the effects of the acoustics alone on the system in question. This approach only considers forward coupling, thus the influence of the sound on the flow field is assumed to be negligible[1].

When applying the hybrid approach, the flow simulation may be solved as compressible or incompressible. Following these results, different analogies may be applied in the aeroacoustic calculations. If a compressible flow simulation has been run, the second spatial derivative of the Lighthill Tensor T_{LH} [2] may be used as the acoustic source term

$$\frac{1}{c_0^2}\frac{\partial^2 p'}{\partial t^2} - \Delta p' = \nabla \cdot \nabla \cdot T_{\mathrm{LH}}, \tag{1}$$

which is valid for a wide range of flows and computes the acoustic pressure in the far field. In (1), c_0 is the reference speed of sound, t is the time and, as mentioned above, p' is a superposition of both the fluid and acoustic pressures. For the incompressible flow case [2] the source term becomes

$$\nabla \cdot \nabla \cdot T_{\mathrm{LH}} = -\Delta p^{\mathrm{ic}} \tag{2}$$

where p^{ic} is the incompressible, or purely hydrodynamic, pressure. Additionally for the incompressible flow case, the perturbations equations [3]may be applied. Using a perturbation ansatz according to [4]

$$p = \bar{p} + p' = \bar{p} + p^{\mathrm{ic}} + p^{\mathrm{a}} \tag{3}$$

which splits the overall pressure into the mean pressure $\bar{p}$, the fluctuating incompressible pressure p^{ic} and acoustic pressure p^{a}. When this splitting is applied to the conservation equations and using $p' = c_0^2\rho' + \text{const.}$ as well as $\nabla \cdot \bar{\mathbf{u}} = 0$ the following relations results [4, 5]

$$\frac{\partial \mathbf{u}^{\mathrm{a}}}{\partial t} + (\bar{\mathbf{u}} \cdot \nabla)\mathbf{u}^{\mathrm{a}} + (\mathbf{u}^{\mathrm{a}}.\nabla)\bar{\mathbf{u}} + \frac{1}{\rho_0}\nabla p^{\mathrm{a}} = 0 \tag{4}$$

$$\frac{1}{\rho_0 c_0^2}\left(\frac{\partial p^{\mathrm{a}}}{\partial t} + \nabla \cdot (p^{\mathrm{a}}\bar{\mathbf{u}})\right) + \nabla \cdot \mathbf{u}^{\mathrm{a}} = \frac{1}{\rho_0 c_0^2}\frac{Dp^{\mathrm{ic}}}{Dt}, \tag{5}$$

where $\bar{\mathbf{u}}$ is the mean flow and $\mathbf{u}^{\mathrm{a}}$ is the acoustic particle velocity. In order to avoid simplification flaws of a neglected mean flow field and a second time derivative which is sensitive to numerical noise errors [6], a scalar acoustic potential is introduced by $\mathbf{u}^{\mathrm{a}} = -\nabla\phi^{\mathrm{a}}$, which after simplification results in the convected wave equation

$$\frac{1}{c_0^2}\frac{D^2\phi^{\mathrm{a}}}{Dt^2} - \nabla \cdot \nabla\phi^{\mathrm{a}} = -\frac{1}{c_0^2}\frac{Dp^{\mathrm{ic}}}{Dt}. \tag{6}$$

In this study, the hybrid approach will be applied. Both compressible and incompressible simulations have been computed in order to conduct the further acoustic analysis. Different source terms, and thus acoustic analogies, have been used and the resulting acoustic pressures obtained in each case will be compared.

CFD Simulations

Both compressible and incompressible CFD simulations have been conducted on the chosen system with air at 10bar and 20 °C using a Detached Eddy Simulation model. The chosen simulation software was StarCCM+ v9.02.007 with double precision and the simulations were conducted on the Vienna Scientific Cluster.

The mesh was resolved with between 1 mio. and 2.5 mio. polyhedral elements. The polyhedral elements greatly increased the convergence time of the simulations and required less mesh elements as, for example, a hexagonal mesh. Mesh extrusions were defined at the inlet and outlet where the mesh size was gradually increased over ten element layers. This was deemed to be necessary, especially in the incompressible simulations, to prevent reflections of the turbulent pressure structures at the inlet and outlet boundaries. It was also applied in the compressible simulations. In addition to the mesh extrusions, in the compressible simulation the free stream inlet and oulet boundary conditions were selected. These boundary conditions are non-reflective in 1D and help to reduce any reflections of the resolved acoustic quantities. In the incompressible CFD the free stream boundary condition is not available and thus a velocity inlet and pressure outlet were applied. Any reflection of the flow or acoustic quantities in the CFD simulations can cause major discrepancies in the following acoustic simulations, and it must thus be ensured that the inlet and outlet are seen as never-ending pipe ends. An inlet profile was applied in all cases, which was obtained from a prior periodic flow simulation on the inlet diameter. An initial steady simulation was conducted for 2500 steps to obtain the initial state of the system. From this state, the unsteady Detached Eddy Simulation was started. The time step was chosen between 15μs and 10μs depending on the relevant Reynolds number and the system was allowed to run for an initial 0.3s until it had reached a stabilised state. Thereafter the simulation was run for a further 0.1s, where for every time step the pressure, divergence of the Lighthill tensor and the second spatial derivative of the Lighthill tensor was read out in to a separate file for all fluid elements. The results of the CFD simulations are as expected. The major sources of velocity changes, pressure changes and vortice production are at the bends, junctions and diameter changes. The most turbulent region occurs after the outlet junction once the two flows in the smaller pipes have joined, see Figure 2 for an example. When the two flows meet in the larger pipe a separation region is formed, producing large eddies which travel down the pipe.

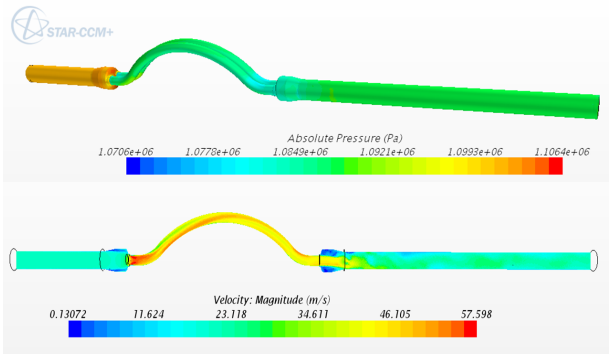

Figure 2: Graphical representation of the flow pressure and velocity at the end time step of an example simulation.

Additional pressure monitoring points were placed at certain locations of the pipe system. When taking Fourier transform of these pressures over time, certain frequency peaks are distinguishable, as shown in Figure 3 for the smallest Reynolds number of 700.000. The pressure level of the compressible simulation lies higher than the incompressible simulation, and also contains more frequency peaks. This is physically correct since both the flow and acoustic pressures are present in the compressible simulation, whereas the incompressible simulation, where the acoustics cannot propogate, contains only the pressures from the flow. The same frequency spectrums were obtained at all Reynolds numbers, with slight shifting in the frequencies and amplitudes, which is most probably due to the increased flow rates, see Figure 4.

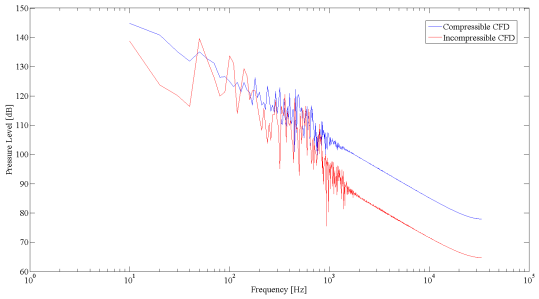

Figure 3: Fourier transform of the inlet monitoring point for compressible and incompressible flow simulations at Reynolds number 700.000.

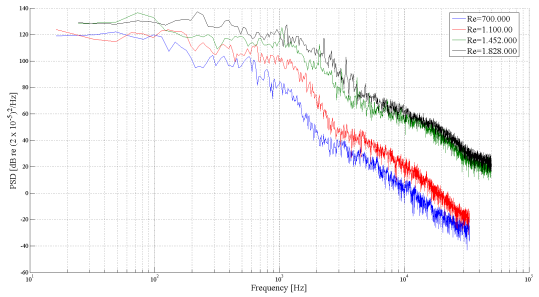

Figure 4: Comparison of frequency spectrums for the incompressible flow simulations at all calculated Reynolds numbers.

Acoustic Simulations

Once the CFD simulations are complete, the source terms are computed on the flow grid and need to be interpolated on to an acoustic mesh for the acoustic analysis. The acoustic mesh is coarser than the CFD mesh, with 86.000 tetrahedral elements. In addition to the current geometry, two further boundary regions must be defined at the inlet and outlet of the pipe. These two regions act as perfectly matched layers for the absorption of the acoustic waves in all directions at the inlet and outlet [7]. This ensures that there are no unrealistic reflections back into the system. The software used, both for the source term interpolation and acoustic simulation, is the multi-physics Finite-Element (FE) based in-house tool CFS++ [2]. The output of the simulation is the acoustic pressure over the fluid volume, which may be viewed using a post-processer in the time or frequency domain. Additionally, the same monitoring points used in the CFD simulation were specified in order to verify the pressure level in the results. Initially three different acoustic source terms were investigated, namely the Laplacian of the incompressible pressure Δp^{ic}, the divergence of the Lighthill tensor $\nabla \cdot T_{\mathrm{LH}}$ and the first time derivative of the incompressible pressure $\frac{1}{c_0^2}\frac{Dp^{\mathrm{ic}}}{Dt}$. In all cases, the main acoustic source at every time step and frequency occurs at the outlet junction of the system, see Figure 5 for an example. This is the area where the most turbulence was seen in the CFD simulations.

The acoustic results required using the Laplacian of the incompressible pressure Δp^{ic} and the divergence of the Lighthill tensor $\nabla \cdot T_{\mathrm{LH}}$ were not as expected. Although the peaks in the pressure spectrum lay at the correct frequencies, the amplitudes lay at a positive offset much higher than expected. The frequency spectrum obtained from the pressure monitoring points using (6) produced much better results, as shown in Figure 6.

Figure 5: A countour plot showing the location of the maximum amplitude of an example acoustic source term at the outlet.

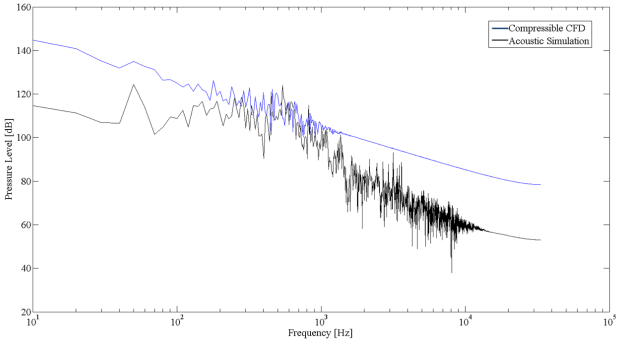

Figure 6: Frequency spectrums of the same pressure monitoring point in the acoustic analysis and compressible CFD simulation.

When comparing the pressure amplitudes to those obtained in the compressible CFD simulations, the acoustic simulation using (6) produces amplitudes slightly below those obtained in the compressible CFD. This result is in full accordance to physics, since the acoustic simulation computes the pure acoustic pressure p^{a} while the compressible CFD results in pressure p', which is a superposition of both the fluid and acoustic pressure. On closer inspection, the major frequency peaks present in the spectrums tend to correspond to the geometrically dependent acoustic resonances in the system. It is thus presumed that the acoustic source at the outlet junction acts as a broadband noise source. This excites, depending on the geometry of the system, different acoustic resonances. For example the frequency peak at 280Hz may correspond to the acoustic resonance present in the smaller pipes. Additionally, the large frequency peak at 550Hz corresponds to the second asymmetrical acoustic resonance of the system between the two junctions, see Figure 7.

These simulated results correlate well with physical measurements performed on a similar system on a gas calibration rig. In these verification measurements the pipe surface velocities of the same pressure monitoring points

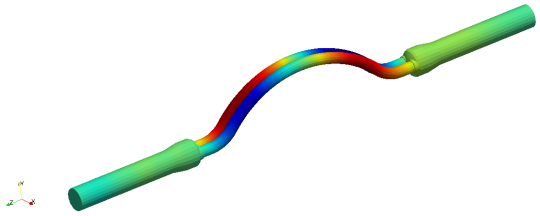

Figure 7: Acoustic pressure mode at 550Hz corresponding to the second asymmertrical acoustic resonance of the system.

as specified in the CFD and acoustic simulations were recorded simultaneously with laser vibrometers. The frequency spectra of this surface velocity, as shown in Figure 8, show similar frequency peaks. The amplitudes of the signals, however, cannot be compared.

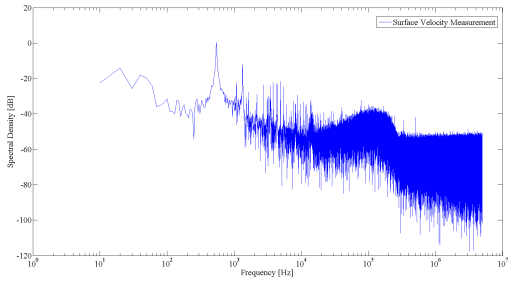

Figure 8: Frequency spectrum of the surface velocity of specified monitoring points as measured on a calibration rig using laser vibrometers.

Conclusion and Future Work

This research has compared results of the acoustic analysis obtained by compressible and incompressible fluid simulations with focus on the identification and quantification of acoustically relevant flow structures. In the case of a geometry containing various obtrusions including junctions, bends and diameter changes, the main acoustic source has been identified at the junction outlet with the acoustic source amplitudes due to the bends and diameter changes minimal in comparison. It has been further discovered that according to which acoustic source term formulation is applied, differing pressure amplitudes can result. In the case of a pipe geometry such as the one used in this analysis, the first time derivative of the incompressible pressure produced the correct results. The pressure frequency spectrum obtained from the acoustic simulations correlated well with the verification measurements, showing the same frequency peaks. In the investigated system it can be concluded that the main acoustic source at the outlet acts as a broadband noise source, which then excites the appropriate acoustic resonances according to the geometry of the pipe. The amplitudes of the acoustic pressures in the system are large enough to cause mechanical vibrations in the system. Further investigations will involve a coupled acoustic-mechanical simulation of the geometry in order to establish the magnitude of the produced vibrations.

Acknowledgements

The computational results presented have been achieved in part using the Vienna Scientific Cluster (VSC). The CFD simulations have been made possible with the provision of a StarCCM+ academic license.

References

[1] C. Wagner, T. Huettl, and P. Sagaut (eds.), *Large-Eddy Simulation for Acoustics*. Cambridge University Press, 2007.

[2] M. Kaltenbacher, *Numerical Simulation of Mechatronic Sensors and Actuators - Finite Elements for Computational Multiphysics*. Springer, 3rd ed., 2015.

[3] R. Ewert, W. Schroeder, *Acoustic Perturbation Equations based on Flow decomposition via Source Filtering*. Journal of Computational Physics 188 (2003), 365398.

[4] A. Hueppe, M. Kaltenbacher, *Spectral Finite elements for computational aeroacoustics using acoustic pertrubation equations*. Journal of Computational Acoustics 20 (2012)

[5] A. Hueppe, *Spectral Finite Elements for Acoustic Field Computation*. Ph.D. thesis, Alpen-Adria-Universitaet Klagenfurt, Austria 2013.

[6] A.Hueppe, J.Grabinger, M.Kaltenbacher, A.Reppenhagen, G.Dutzler, W.Kuehnel, *A Non-Conforming Finite Element Method for Computational Aeroacoustics in Rotating Systems*. 20th AIAA/CEAS Aeroacoustics Conference, 2014.

[7] B.Kaltenbacher, M.Kaltenbacher, *I.Sim: A modified and stable version of a perfectly matched layer technique for the 3-d second order wave equation in time domain with an application to aeroacoustics*. Journal of Computational Physics, 2013.